JOC The Journal of Organic Chemistry

Article

pubs.acs.org/joc

π-Expanded Dipyrrolonaphthyridinediones with Large Two-Photon Absorption Cross-Section Values

Bartłomiej Sadowski,[†] Hanayo Kita,[‡,§] Marek Grzybowski,[†] Kenji Kamada,*[,‡,§] and Daniel T. Gryko*[,†]

[†]Institute of Organic Chemistry, Polish Academy of Sciences, Kasprzaka 44/52, 01-224 Warsaw, Poland

[‡]IFMRI, National Institute of Advanced Industrial Science and Technology (AIST), AIST Kansai Centre, Ikeda, Osaka 563-8577, Japan

[§]Department of Chemistry, School of Science and Technology, Kwansei Gakuin University, Sanda, Hyogo 669-1337, Japan

Supporting Information

ABSTRACT: A synthetic entry to novel dyes based on the dipyrrolonaphthyridinedione core was developed via the Heck reaction. These weakly fluorescent compounds bearing double bond linkages between the core and the peripheral units absorbed strongly in the far-red/NIR region and possessed large values of two-photon absorption (TPA) cross-sections (up to 5180 GM). Additionally, analogous dyes bearing triple bond linkages were also efficient TPA materials with relatively large two-photon absorption cross-sections (up to 2840 GM) as well as two-photon brightness (up to 1450 GM). The centrosymmetric nature of both of these families of dyes is responsible for the location of the maxima of two-photon absorption being at much higher energy than the ones corresponding to the double wavelength of the lowest-energy one-photon absorption. Theoretical calculations clarified that the enhancement of the TPA by the peripheral substitutions arose through different mechanisms depending on either the electron-donating or electron-withdrawing ability of a given substituent to the ambipolar core. The change in the electron distribution of HOMO and HOMO−1 by the push−pull effect was found to govern the strength of the lowest-energy TPA-allowed transition. Importantly, compounds from both series possessed a beneficial ratio of σ_2/MW (1.6−9.8 GM/g).

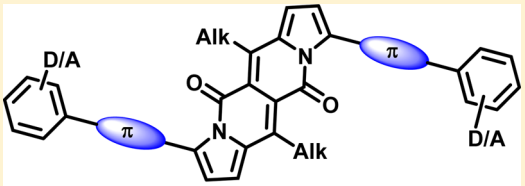

π		
λ_{TPA}^{max} [nm]	740-820	720-860
σ_2 [GM]	1710-5180	850-2840
σ_2/M [GM/g]	3.2-9.8	1.6-5.1

INTRODUCTION

Multiphoton processes have been a topic of continuous interest since the 1960s, but the invention of two-photon fluorescence microscopy gave the strongest impetus to this field.[1] Chromophores possessing large two-photon absorption cross-section (σ_2) values combined with useful secondary features have found many biologically-oriented applications, e.g., imaging of deeper-located tissues[2] and mitochondria in cells,[3] ion sensing,[4] as well as probes for hydrogen sulfide,[5] nitric oxide,[6] hydrogen peroxide,[7] β-amyloid plaques,[8] or biothiols.[9] Two-photon absorption (TPA) has also found many applications in various fields of science, such as photodynamic therapy,[10] two-photon-induced photopolymerization (TPIP),[11] optical power limiting,[12] measurement of a molecular electric field,[13] three-dimensional data storage,[14] or three-dimensional lithography.[15] From a structural point of view, various chromophores have been utilized as a core for such materials, including stilbene,[16] fluorene,[17] coumarins,[18] porphyrins,[19] diradicals,[20] and radical cations.[21] Three basic structural motifs have been employed, so-called dipolar,[22] quadrupolar[16b,23] or octupolar,[24] to design chromophores with enhanced σ_2 in the visible and near-IR ranges of wavelengths. Large TPA cross-sections have also been associated with efficient π-delocalization within an extended π-conjugated system. In this fashion, many π-conjugated, quadrupolar-type systems containing double or triple bond linkages between the core and either the donor or the acceptor units have been designed and their TPA properties have been examined.[25] The selected examples of such dyes are shown in Figure 1. In 2003, Cho's group described a series of quadrupolar-type anthracene derivatives enlarged by electron-rich arylethenyl units.[26] It was shown that incorporation of an electron-accepting group (CN) into the positions 9 and 10 caused a red shift of the TPA maxima, as well as a 2-fold enhancement of the TPA cross-section value. A few years later, compounds containing an electron-rich core and electron-accepting units as the peripheral groups were developed by Marder's group.[27] These molecules exhibited strong TPA response in the range of 1050−1250 nm. In 2015, we synthesized a series of quadrupolar dyes based on an electron-poor diketopyrrolopyrrole core bearing imidazolethynyl units.[28] The obtained salts, thanks to a strong TPA response in DMSO and pure water, were applied as probes for selective staining of mitochondria in two-photon fluorescence microscopy.

Recently, we have introduced a completely new heterocyclic chromophore, namely, dipyrrolonaphthyridinedione (DPND), which can be readily synthesized in two steps from simple

Received: April 9, 2017
Published: June 28, 2017

DOI: 10.1021/acs.joc.7b00831
J. Org. Chem. 2017, 82, 7254−7264

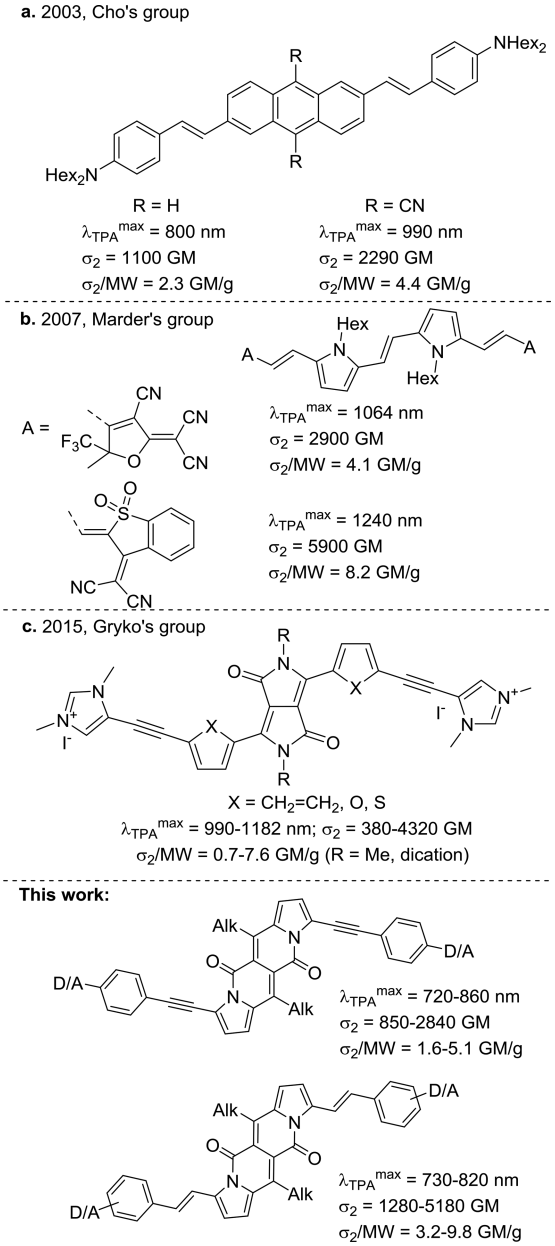

Figure 1. Examples of quadrupolar TPA dyes.

starting materials.[29] DPND derivatives exhibit promising photophysical properties: strong absorption in the visible range and high fluorescence quantum yields. Moreover, owing to its cross-conjugated nature, the DPND core shows ambipolar character: it may serve both as a donor in A−D−A quadrupolar dyes, as well as an acceptor in D−A−D quadrupolar dyes. We envisioned, based on our previous research devoted to quadrupolar-type diketopyrrolopyrroles[28,30] or pyrrolo[3,2-*b*]pyrroles,[31] that this type of skeleton enlarged by two arylethenyl or arylethynyl units at each side could also possess intriguing nonlinear characteristics.

Herein, we report the synthesis of several quadrupolar-type chromophores containing the DPND skeleton via Heck coupling. The ambipolar character of the DPND core prompted us to perform investigations of linear and nonlinear optical properties of the synthesized compounds, as well as dyes that had been previously prepared bearing triple bond linkages[29] that take into consideration both electron donors (OMe, NMe_2) and acceptors (CN, NO_2) as peripheral groups. Furthermore, we also conducted the computational studies on the two-photon absorption properties of the quadrupolar chromophores to understand the influence of the peripheral substituent groups and the π-conjugation linkers on the optical properties and the mechanisms.

RESULTS AND DISCUSSION

Design and Synthesis. Dialkyl DPND derivatives can be readily synthesized by the condensation of intermediate **1** with aliphatic carboxylic acids, as was demonstrated in our previous report (Scheme 1).[29] In order to increase the solubility of the

Scheme 1. Synthesis of Compound 3

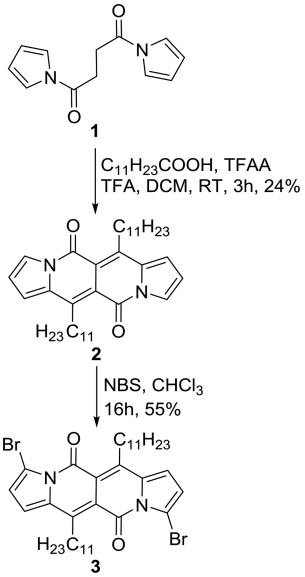

final dyes, we decided to use lauric acid as the starting material, which should result in DPNDs bearing *n*-undecyl groups at positions 6 and 12. Hence, stirring the intermediate **1**[29] with lauric acid, trifluoroacetic anhydride (TFAA), and trifluoroacetic acid (TFA) in DCM at room temperature smoothly yielded di-*n*-undecyl DPND **2**, which was subsequently brominated by means of NBS under the standard conditions.

Then, compound **3** was subjected to the classical Heck coupling protocol [$Pd(OAc)_2$, P(*o*-tolyl)$_3$, Et_3N, DMF, 100 °C, 24 h]. This reaction resulted in the formation of compound **4a** only in 10% yield (Table 1, entry 1). Conducting the reaction at lower temperature (90 °C) and using a higher-boiling base (*N*,*N*-diisopropylethylamine, DIPEA) led to the target compound in 25% yield (Table 1, entries 2 and 3). A further increase in the amounts of styrene and base led to a significant increase in the yield of the reaction (Table 1, entry 4). Taking into consideration the fact that the product of a single Heck reaction can precipitate during the reaction due to intensified π-stacking interactions, we also increased the quantity of solvent and obtained dye **4a** in 50% yield (Table 1, entry 5). The best result was obtained for the reaction in which a large excess of base was added, and again, a higher amount of solvent was used; the yield of product **4a** was improved to 56% (Table 1, entry 6). Further increasing the amount of solvent slightly decreased the yield of the desired compound (Table 1, entry 7). However, when we used toluene as a solvent (Table 1, entry 8)

DOI: 10.1021/acs.joc.7b00831
J. Org. Chem. 2017, 82, 7254−7264

Table 1. Optimization of the Heck Coupling Conditions

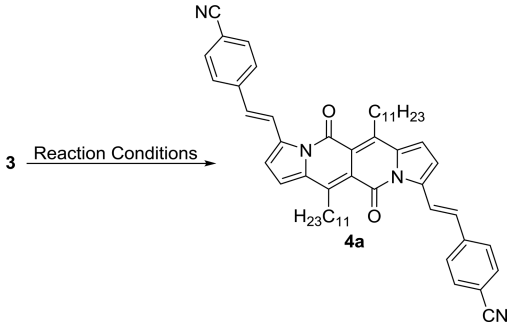

	reaction conditions[a]					
entry	styrene (equiv)	ligand (20%$_{mol}$)	base (equiv)	solvent	temp (°C)	yield of **4a** (%)[b]
1	3	P(*o*-tol)$_3$	Et_3N (3)	DMF (2 mL)	100	10
2	3	P(*o*-tol)$_3$	Et_3N (3)	DMF (2 mL)	90	18
3	3	P(*o*-tol)$_3$	DIPEA (3)	DMF (2 mL)	90	25
4	4	P(*o*-tol)$_3$	DIPEA (4)	DMF (2 mL)	90	45
5	4	P(*o*-tol)$_3$	DIPEA (4)	DMF (4 mL)	90	50
6[c]	**4**	**P(*o*-tol)$_3$**	**DIPEA (0.1 mL)**	**DMF (6 mL)**	**90**	**56**
7	4	P(*o*-tol)$_3$	DIPEA (0.1 mL)	DMF (7 mL)	90	54
8	3	P(*o*-tol)$_3$	Et_3N (3)	PhMe (2 mL)	90	6
9	3	IMes·HCl	Cs_2CO_3 (3)	DMAc (2 mL)	90	0

[a]$Pd(OAc)_2$ (10%$_{mol}$) was used as a catalyst in all cases. [b]Isolated yields. [c]The bold entry signifies the optimal conditions.

or IMes·HCl as a ligand precursor[32] (Table 1, entry 9), we obtained either only traces or no product, respectively.

After the optimal conditions (Table 1, entry 6) were established for the desired transformation, the scope and limitations of this approach were investigated by testing a variety of styrenes (Table 2). Using 4-nitrostyrene or 3-methoxystyrene as a coupling partner, we obtained the corresponding dyes **4b** and **4c** in 18% and 51% yield, respectively. The low yield in the case of **4b** was caused by the low solubility of the dye, as well as quite a complex reaction outcome. Applying 4-methylstyrene, 4-methoxystyrene, or 4-dimethylaminostyrene resulted in the formation of complicated and unseparable mixtures (Table 2, entries 4–6).

Table 2. Synthesis of Dyes 4a–4c

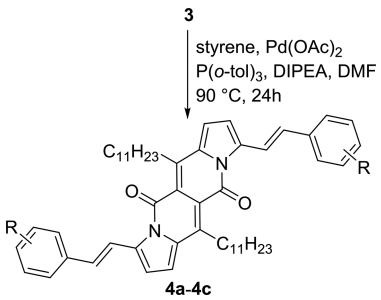

entry	R	product	yield (%)[a]
1	*p*-CN	**4a**	56
2	*p*-NO_2	**4b**	18
3	*m*-OMe	**4c**	51
4[b]	*p*-OMe		
5[b]	*p*-NMe_2		
6[b]	*p*-Me		

[a]Isolated yields. [b]A complicated, unseparable mixture was obtained.

Linear Optical Properties. We have performed optical studies both for dyes **4a–4c** as well as for analogous DPNDs containing arylethynyl substituents (**5a–5c**) prepared earlier (Figure 1, Table 3).[29] The UV–visible absorption (i.e., one-photon absorption, OPA) and (OPA-induced) fluorescence spectra of compounds **4a–4c** and **5a–5c** are shown in Figure 2, and the spectroscopic parameters of the linear and nonlinear optical properties are summarized in Table 3. The absorption spectra of DPND-based dyes **4a–4c** show two pronounced bands (similar to those of **5a–5c**): a short-wavelength band with a maximum localized in the range of 300–400 nm and a long-wavelength band localized in the far-red region (603–621 nm). The positions of the long-wavelength absorption bands of **4a–4c** were red-shifted by ~85–125 nm in comparison with previously described, nonsubstituted DPND[29] and depended strongly on the electron-accepting ability of the peripheral unit. Treating *m*-OMe substituent as "neutral", the absorption maxima were more red-shifted as the electron-accepting ability of the substituent increased, whereas, rather surprisingly, for compounds **5a–5c** this relationship was reversed. Weak conjugation between the meta-located methoxy group and the central core in **4c** was reflected in the lowest molar absorption coefficient (55 100 $M^{-1}\cdot cm^{-1}$) of the long-wavelength band, albeit the highest value of ε (60 200 $M^{-1}\cdot cm^{-1}$) was noted for compound **4b**, highlighting the presence of strong conjugation between the DPND core and the NO_2 group. For compounds with a triple bond linkage, nitro-substituted **5a** possessed the highest value of molar absorption coefficient (57 300 $M^{-1}\cdot cm^{-1}$), but compound **5c**, containing a highly electron-rich peripheral unit, exhibited a comparable ε.

The fluorescence maxima of **4a–4c** were located in the deep-red region (662–699 nm) and they were bathochromically shifted relative to those of **5a** and **5b**, while the emission maxima of dye **5c** was located in the NIR region (736 nm). Dyes **4a–4c** possessed moderate Stokes shift values (1500–1800 cm^{-1}), suggesting a small conformational change in the

DOI: 10.1021/acs.joc.7b00831
J. Org. Chem. 2017, 82, 7254–7264

Table 3. Linear and Nonlinear Optical Properties of Compounds 4a–4c and 5a–5c Measured in Dichloromethane

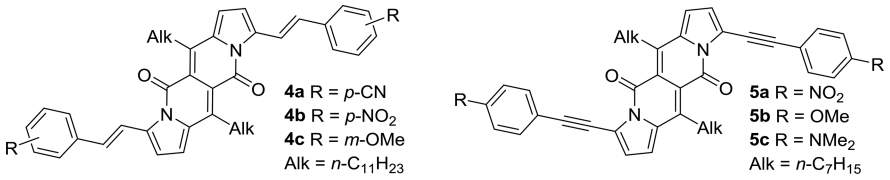

dye	λ_{abs}^{max} [nm]	$10^{-3}\cdot\varepsilon_{max}$ [$M^{-1}\cdot cm^{-1}$]	λ_{em}^{max} [nm]	Φ_{fl} [b]	$\delta\nu$ [cm^{-1}] [a]	λ_{TPA}^{max} [nm]	σ_2 [GM] (±error)	$\sigma_2\cdot\Phi_{fl}$ [GM]	σ_2/MW [d] [GM/g]
4a	326, 610	52.7, 56.3	671	0.022	1500	740	5100 (700)	112	9.8
4b	326, 372, 621	41.5, 31.0, 60.2	699	0.016	1800	820	5180 (670)	83	9.3
4c	312, 603	58.6, 55.1	662	0.041	1500	740	1710 (210)	70	3.2
5a [c]	355, 599	27.3, 57.3	633	0.51	900	720	2840 (340)	1450	5.1
5b [c]	302, 601	47.5, 52.4	643	0.59	1100	720	850 (150)	500	1.6
5c [c]	303, 645	61.0, 56.6	736	0.17	1900	860	1990 (330)	340	3.6

[a]Stokes shift, i.e., the difference between the lowest-energy absorption band and the highest-energy emission band expressed in cm^{-1}. [b]Cresyl violet was used as a reference (Φ_{fl} = 0.54 in MeOH). [c]The linear optical data are taken from ref 29. [d]The molecular weights were calculated by assuming Alk = Me.

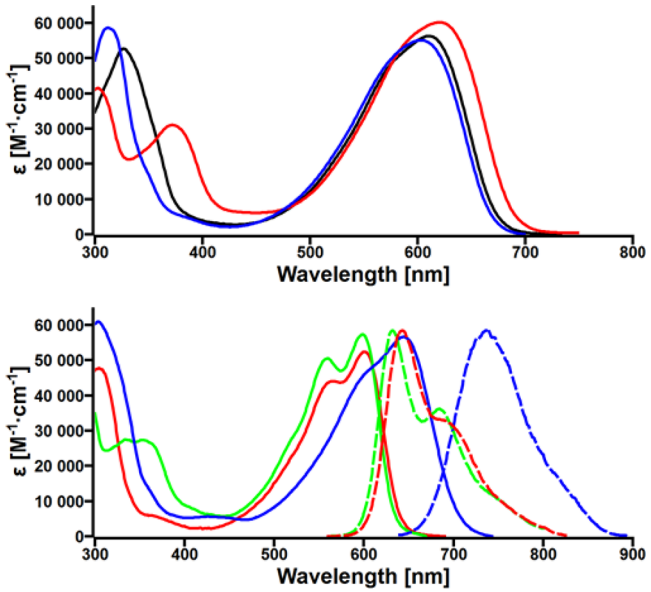

Figure 2. (Top) Absorption spectra of compounds **4a** (black), **4b** (red), and **4c** (blue). (Bottom) Absorption (solid) and normalized emission (dotted) spectra of compounds **5a** (green), **5b** (red), and **5c** (blue).

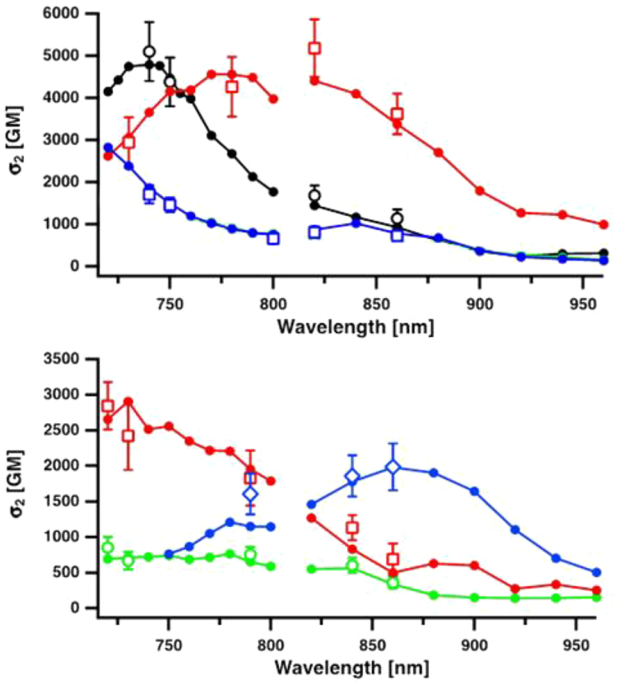

Figure 3. (Top) Two-photon absorption spectra of compounds **4a** (black), **4b** (red), and **4c** (blue) in dichloromethane. (Bottom) Two-photon absorption spectra of compounds **5a** (red), **5b** (green), and **5c** (blue). The data were obtained by different experimental procedures, with the filled circles representing data obtained for a fixed incident power and the open symbols representing data obtained by power-dependence experiments of the incident beam.

excited state. The fluorescence quantum yields (Φ_{fl}) of **4a–4c** were significantly lower (0.022–0.041) compared to those of compounds **5a–5c** (0.17–0.51), which may be attributed to the presence of an additional de-excitation mechanism involving *E–Z* isomerization of double bonds.[33] The emission is the strongest in the case of dye **4c**, bearing a meta-located methoxy group, and the lowest in the case of dye **4b**, which is in accordance with the usual emission quenching effect of a NO_2 group. In contrast, this effect did not apply for dye **5a**, which exhibited a surprisingly high Φ_{fl} of 0.51. Functional dyes bearing nitro groups and fluorescence quantum yields on this level have been sparsely reported in the literature.[34]

Two-Photon Absorption Properties. TPA spectra of the dyes **4a–4c** and **5a–5c** were measured in dichloromethane from 720 to 960 nm (Figure 3) by using the femtosecond open-aperture Z-scan method.[35,36] In Figure 3, data points of TPA cross-section (σ_2) obtained by different experimental procedures of the Z-scan measurements are indicated with different symbols. Data were obtained either by using a fixed incident power or by experiments based on the power-dependence of the incident beam, which ensured the assignment of observed signals to the TPA process and gave more accurate values of σ_2 with experimental error. Typical open-aperture Z-scan traces observed with various incident powers are shown in Figures S1 and S2 in Supporting Information.

The compounds were found to have strong two-photon absorption in the measured spectral range. All compounds except for **5b** had σ_2 values exceeding 1000 GM (where GM is the unit of the TPA cross-section and 1 GM = $10^{-50}\cdot cm^4\cdot s$

DOI: 10.1021/acs.joc.7b00831
J. Org. Chem. 2017, 82, 7254–7264

photon^{-1}·molecule^{-1}) at some wavelengths. The maximum values of σ_2 are summarized in Table 3. Interestingly, the shape of the TPA spectra considerably differed from one compound to another. Compound **4a** (R = *p*-CN) showed a TPA maximum at 740 nm and the tail extended to ca. 900 nm, while compound **4b** (R = *p*-NO_2) showed a red-shifted, much broader peak centered at around 820 nm. These two compounds, having strong peripheral acceptors, were found to have very large σ_2 values (σ_2 = 5100 ± 700 GM for **4a** and σ_2 = 5180 ± 670 GM for **4b**, obtained by the power-dependence experiments). The TPA spectra of compound **4c** (R = *m*-OMe) was blue-shifted compared to those of **4a** and **4b**, and the maximum was located at a wavelength shorter than 720 nm. The highest observed σ_2 value for this dye was still large (σ_2 = 1710 GM) but significantly smaller when compared to those of **4a** and **4b**. Therefore, the introduction of strong electron accepting groups (CN and NO_2) into the DPND framework was more effective to enhance TPA in the NIR region than was the use of weak donors (OMe), indicating better electronic communication in DPND-based A−D−A dyes through the strong push−pull effect over the π-conjugation. The NO_2 groups of **4b** can couple with the π-conjugation of the arylethenyl arms through the DPND core. This leads to a decrease of the energy level, resulting in a significant red shift of the TPA band compared to that of **4a**.

Two of the compounds having arylethynyl arms (**5a**, R = *p*-NO_2 and **5b**, R = *p*-OMe) exhibited a similar spectral shape as **4c**, but with broader peaks. When compounds possessing the similar peripheral units (*p*-NO_2 and *p*-/*m*-OMe) were compared, the magnitude of **5a** was roughly 3 times as large as that of **5b**, which is similar to the relation between **4b** and **4c**. As in the case of **4b** and **4c**, the presence of a strongly electron-withdrawing NO_2 group led to large σ_2 values due to the strong A−D−A quadrupolar nature of the resulting chromophore. The spectral shape of **5a** can be understood as the blue-shifted one of **4b** (by ∼100 nm). The maximum value of σ_2 for **5a** was 2840 ± 340 GM and was smaller than that of **4b**. A similar trend was also observed for **4c** and **5b**, both having a OMe group, with ethynyl-bridged dye **5b** displaying a significantly lower TPA cross-section. This behavior, i.e., a decrease in σ_2 and a blue shift of the TPA maxima, obtained by changing from arylethenyl groups to arylethynyl ones, can be explained by the difference in the strength of π-conjugation between double and triple bonds. As shown by Meier,[37a] Blanchard-Desce and co-workers,[37b] and Kamada et al.,[37c] the ethylene linker ensures better conjugation between various parts of the molecule, leading typically to a stronger bathochromic shift, larger two-photon absorption cross-section, etc. Taking into account the expected blue shift with the triple bond, the peak wavelength (860 nm) of the broad TPA band of compound **5c** (R = *p*-NMe_2) can be recognized as an extraordinary red shift, although the peak σ_2 is smaller than that of **4a**.

Two-photon brightness (or action cross-section, $\sigma_2 \cdot \Phi_{fl}$) is an important parameter from the practical point of view in bioimaging applications. Compounds **4a**−**4c** have high σ_2 values (1710−5180 GM), but due to low fluorescence quantum yields (0.022−0.041), their two-photon brightness is relatively low (70−112 GM, Table 3). On the other hand, compounds **5a**−**5c** exhibit a high two-photon brightness of 340−1450 GM because of the high Φ_{fl} of 0.17−0.51 and the relatively high σ_2 of 950−2850 GM. The high two-photon brightness of DPNDs **5a**−**5c** is comparable to those of π-extended diketopyrrolopyrroles.[28,30a]

The TPA cross section value scaled to its molecular weight (σ_2/MW) is a simple but useful measure for TPA activity. High values of σ_2/MW are very beneficial from the point of view of various applications. This fact is related to both an increase of solubility problems and problematic cell permeability, as well as synthetic difficulties, in cases when σ_2/MW is low. In many cases, an increase of the TPA cross-section value is strongly connected with an enlarged π-conjugation within the molecule and hence the increase of its molecular weight. That is why the σ_2/MW ratio usually remains almost unchanged. During our studies we observed that compounds **4a** and **4b** displayed a high factor of σ_2/MW (9.8 and 9.3 GM/g, respectively). These values, as well as TPA cross-sections of DPND-based compounds, were in good agreement with those for quadrupolar-type ones synthesized by Marder's group[27] (Figure 1) or Cho's group (λ_{TPA}^{max} = 980 nm, σ_2 = 5530 GM, σ_2/MW = 7.65 GM/g),[38] although the TPA maxima of these molecules were blue-shifted. Taking into consideration larger molecules, similar σ_2/MW factors were obtained for porphyrin tape consisting of two porphyrin units (λ_{TPA}^{max} = 1200 nm, σ_2 = 11900 GM, σ_2/MW = 9.49 GM/g)[19a] or the D−π−A-type molecule with porphyrin as a core and peripheral azulene units (λ_{TPA}^{max} = 1400 nm, σ_2 = 8030 GM, σ_2/MW = 7.60 GM/g).[39] Large TPA cross-section values for the above-mentioned porphyrin derivatives were overcome by their high molecular weights, therefore causing contraction of the σ_2/MW ratio.

For all compounds, the observed TPA band (720−900 nm) had a transition energy (2.75−3.44 eV) located between those of the lowest (595−645 nm, 1.92−2.08 eV) and the second-lowest OPA peaks (302−372 nm, 3.33−4.11 eV), as shown in Figures S3 and S4 in the Supporting Information. These results show that TPA and OPA bands of the compounds have complementary behavior and that the molecules obeyed the symmetry selection rules of the optical transition, as expected from their centrosymmetric molecular design. Thus, the destination states of the TPA transitions are the higher excited states inaccessible by OPA, as also supported by the theoretical calculations shown in the following sections.

Simulation of the TPA Spectra. To obtain deeper insight of the relation between the structures and the TPA properties of the π-extended DPND derivatives, we performed the simulation of the TPA spectrum based on *ab initio* molecular orbital calculation. Five types of donor/acceptor substituents in the para position (including the nonsubstituted) for each π-linker (ethylene and ethynylene), i.e., **4′pNMe$_2$** (R = *p*-NMe_2), **4′pOMe** (R = *p*-OMe), **4′** (R = H), **4′pCN** (R = *p*-CN), and **4′pNO$_2$** (R = *p*-NO_2) for the ethylene-linker system and **5′pNMe$_2$** (R = *p*-NMe_2), **5′pOMe** (R = *p*-OMe), **5′** (R = H), **5′pCN** (R = *p*-CN), and **5′pNO$_2$** (R = *p*-NO_2) for the ethynylene-linker system, were calculated in addition to **4′mOMe** (R = *m*-OMe) to investigate the substitution-position effect. In these molecules, the long alkyl chains were replaced with a methyl group (Alk = Me) to save computation resources. This kind of simplification of long alkyl chains is known to give little influence on the calculation results of optical properties. Geometries were optimized at the CAM-B3LYP//6-31+G(d) level of theory with the polarizable continuum model (PCM) in dichloromethane. The Tamm−Dancoff approximation (TDA)[40] was applied for the same level of theory to calculate the transition energy and the transition dipole moments necessary for the spectral simulation of OPA and TPA.[41]

The simulated TPA spectra (Figure 4) well reproduced the characteristic features of the experimental spectra, although

DOI: 10.1021/acs.joc.7b00831
J. Org. Chem. 2017, 82, 7254−7264

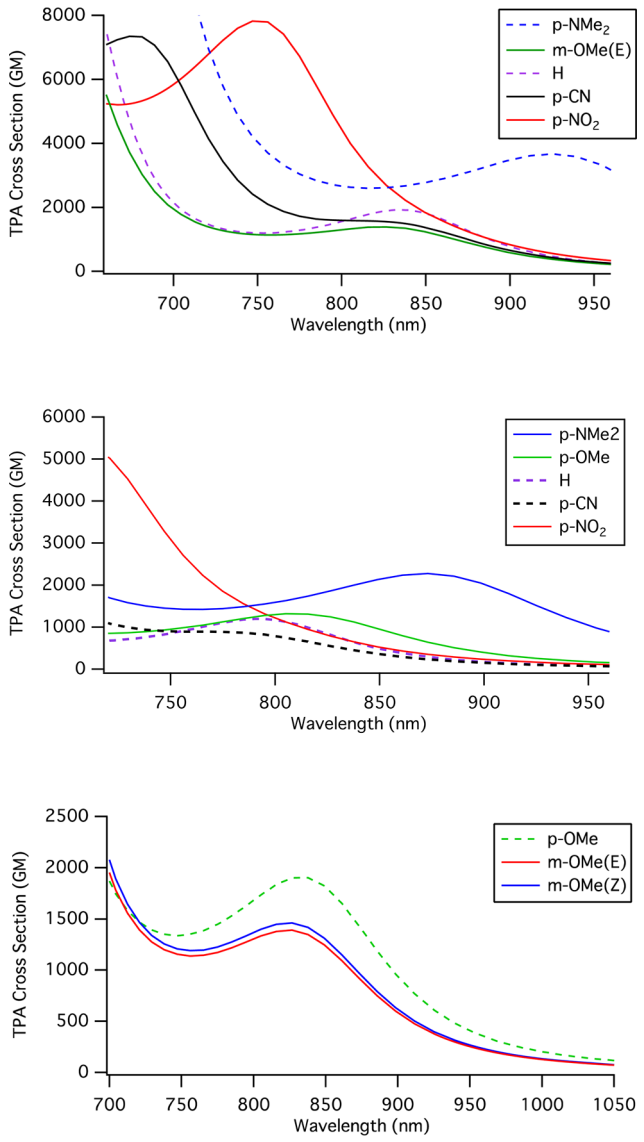

Figure 4. (Top) Simulated two-photon absorption spectra of **4′pNMe$_2$** (blue), **4′mOMe(E)** (green), **4′** (purple), **4′CN** (black), and **4′NO$_2$** (red) calculated at the TDA-CAM-B3LYP/PCM(in dichloromethane)//6-31+G(d) level of theory. The relaxation constants are taken as 0.24 eV. (Middle) The same ones for **5′pNMe$_2$** (blue), **5′pOMe** (green), **5′** (purple), **5′CN** (black), and **5′NO$_2$** (red). (Bottom) The same ones for **4′pOMe** (green) and two geometrical isomers of **4′mOMe(E)/(Z)** (red and blue). Structures are shown in Figure S6 of the Supporting Information. The data that has no corresponding experimental spectra are shown with dashed curves.

they are blue-shifted by ∼50 nm and overestimated the cross section in some measurements. The spectrum of **4′pCN** has an intense peak at 780 nm and a weak peak at 830 nm, resembling the peak with a long tail on the long-wavelength side of the experimental spectrum of **4a** (R = *p*-CN). The spectrum of **4′pNO$_2$** has a single intense peak at 760 nm, like **4b** (R = *p*-NO$_2$). Meanwhile, **4′mOMe** has two geometrical isomers by rotation around the bond between the ethylene and phenyl group. The isomers have the same spectrum with a weak peak at 830 nm and the tail of another peak at the shorter wavelength. This shape again agrees with the experimental spectrum of **4c** (R = *m*-OMe), which has a small peak at 850 nm and the monotonic increase at the short-wavelength side. The similar correspondences between the simulated and experimental spectra were also found for the ethynylene-linked molecules. The intense peak of **5′pNO$_2$** is blue-shifted significantly relative to that of **4′pNO$_2$**, as observed between **5a** (R = NO$_2$) and **4b** (R = *p*-NO$_2$). **5′pOMe** has a weak peak like **5b** (R = OMe). In addition, **5′pNMe$_2$** has a single moderate peak at 870 nm, matching that of **5c** (R = NMe$_2$).

The spectra having no corresponding experimental results are also shown with a dashed curve in Figure 4. The nonsubstituted ethylene π-linker molecule **4′** has almost the same magnitude and peak wavelength as **4′pOMe** has. The molecule **4′pNMe$_2$** has a blue-shifted and more intense peak at 920 nm compared to that of **4′**. The peak of **4′pOMe** is slightly higher than that of **4′mOMe**. The nonsubstituted ethynylene π-linker molecule **5′** has a slightly blue-shifted and weaker peak at 790 nm relative to that of **5c** (R = NMe$_2$). Interestingly, unlike **4′pCN**, the ethynylene π-linker molecule with a CN group, **5′pCN**, is rather weaker than **5′**, although it has a strong acceptor group. In general, the ethylene π-linker molecules (**4′** series) have larger TPA cross sections than the ethylene π-linker molecules (**5′** series) have. However, they show a complicated dependence against the donor/acceptor strength of the substituent.

The complicated dependence can be understood in a organized way by decomposing the overall TPA spectrum into the constituting components by the destination excited state (Figure 5). The calculated transition energy, symmetry, and electronic configuration of some excited states are summarized in Table 4. First, let us concentrate on the molecules having the double-bond π-linker (Figure 5, top row). The $S_0 \rightarrow S_1$ transition is one-photon absorption allowed (A_u-symmetry) transition and TPA forbidden. The first (longest wavelength) TPA peak is the $S_0 \rightarrow S_2$ transition (designated by red arrows and called here the type I transition) for all molecules, although it is covered up by stronger $S_0 \rightarrow S_3$ transition for R = *p*-NO$_2$. The magnitude of the $S_0 \rightarrow S_2$ transition is moderate and decreases from strong donor to neutral (R = H) and to strong acceptor, while the peak wavelength red-shifts by either donor or acceptor substitution from neutral; in particular, the *p*-NMe$_2$ group leads to the largest red shift of all. The $S_0 \rightarrow S_3$ transition is intense and is the main contribution of the first distinguishable peak for R = *p*-NO$_2$ and the second distinguishable peak for R = *p*-CN. The TPA transition, having the same nature as the $S_0 \rightarrow S_3$ transition (named type II and designated by green arrows), also exists as a higher excited state for the donor-substituted and nonsubstituted molecules. The energy level lowers upon increasing the electron-withdrawing ability and plays the dominant role instead of the $S_0 \rightarrow S_2$ transition for the acceptor-substituted molecules. The above discussions are applicable to the results for the molecules having the triple-bond π-linker (Figure 5, bottom row), but the influence of the donor/acceptor substitution is smaller even with the same kind of substituent (for example, the blue shift of the TPA peak of **5′pNO$_2$** from that of **4′pNO$_2$** versus that of **5a** from **4b** in the experimental spectra).

These calculation results explained why flanking the DPND core with both electron-donating and electron-withdrawing groups leads to large TPA cross sections. The electron-donating substitution enhances the strength of the $S_0 \rightarrow S_2$ (type I) transition and the electron-withdrawing substitution lowers the energy of the $S_0 \rightarrow S_3$ (type II) transition. The dependence of

DOI: 10.1021/acs.joc.7b00831
J. Org. Chem. 2017, 82, 7254−7264

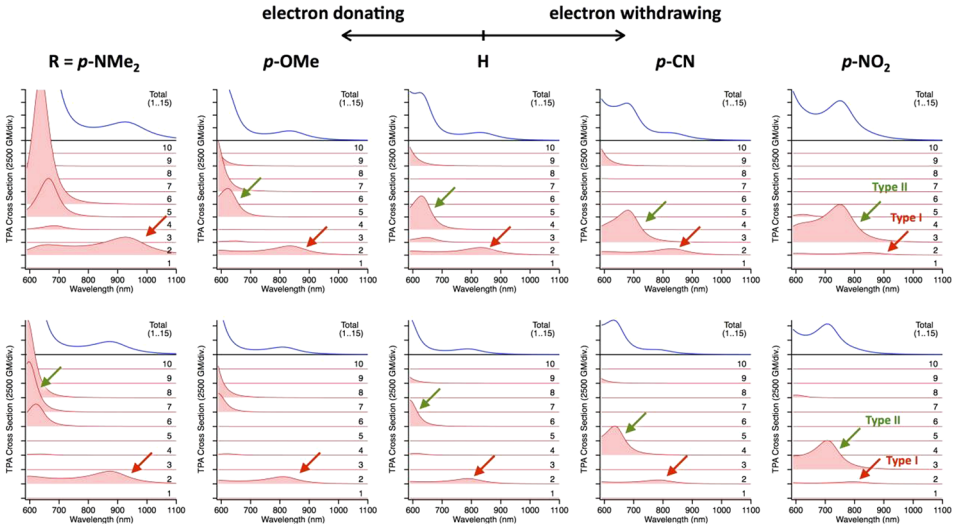

Figure 5. Decomposed TPA spectra by the destination excited state ($S_0 \rightarrow S_n$, where n indicates the excited state; spectra shown in red). Up to 10 of the 15 excited states calculated are shown. The total TPA spectra of the 15 excited states are shown on top of each panel (blue curve). Top row, from left to right: **4′pNMe$_2$**, **4′pOMe**, **4′**, **4′pCN**, and **4′pNO$_2$**. Bottom row, from left to right: **5′pNMe$_2$**, **5′pOMe**, **5′**, **5′pCN**, and **5′pNO$_2$**

Table 4. Symmetry, Transition Energy (wavelength), Electronic Configuration, and Their Contribution of the First Four Excited States of the Model Molecules Calculated at the TDA-CAM-B3LYP/PCM//6-31+G(d) Level of Theory in Dichloromethane

n of S_n	4′pNMe$_2$	4′p OMe	4′	4′pCN	4′pNO$_2$
1	A_u 1.95 eV (636 nm)	A_u 2.17 eV (565 nm)	A_u 2.16 eV (574 nm)	A_u 2.15 eV (577 nm)	A_u 2.11 eV (589 nm)
	H → L 0.67629	H → L 0.68753	H → L 0.69034	H → L 0.68806	H → L 0.67671
2	A_g 2.61 eV (475 nm)	A_g 2.91 eV (429 nm)	A_g 2.93 eV (424 nm)	A_g 2.93 eV (423 nm)	A_g 2.87 eV (432 nm)
	H−1 → L 0.65059	**H−1 → L 0.66095**	**H−1 → L 0.67424**	**H−1 → L 0.66937**	**H−1 → L 0.63154**
3	A_u 3.49 eV (355 nm)	A_g 3.75 eV (336 nm)	A_g 3.76 eV (330 nm)	A_g 3.56 eV (348 nm)	A_g 3.23 eV (383 nm)
	H−2 → L 0.6543	H → L+2 0.60784	**H → L+1 −0.45684**	**H → L+1 0.63053**	**H → L+1 0.58217**
			H → L+2 0.46369		
4	A_g 3.55 eV (349 nm)	A_u 3.88 eV (322 nm)	A_g 3.85 eV (322 nm)	A_g 3.87 eV (320 nm)	A_u 3.48 eV (356 nm)
	H → L+1 0.4632	H−2 → L 0.60306	H → L+2 0.48763	H → L+3 0.66613	H → L+3 0.57635
			H → L+1 0.44611		
n of S_n	5′pNMe$_2$	5′p OMe	5′	5′pCN	5′p NO$_2$
1	A_u 2.13 eV (581 nm)	A_u 2.26 eV (548 nm)	A_u 2.31 eV (536 nm)	A_u 2.31 eV (537 nm)	A_u 2.28 eV (544 nm)
	H → L 0.67467	H → L 0.68861	H → L 0.69193	H → L 0.68981	H → L 0.67641
2	A_g 2.78 eV (446 nm)	A_g 3.00 eV (413 nm)	A_g 3.09 eV (401 nm)	A_g 3.10 eV (400 nm)	A_g 3.06 eV (405 nm)
	H−1 → L 0.67467	**H−1 → L 0.66064**	**H−1 → L 0.6733**	**H−1 → L 0.66968**	**H−1 → L 0.63835**
3	A_u 3.60 eV (345 nm)	A_u 3.85 eV (322 nm)	A_u 3.84 eV (323 nm)	A_u 3.81 eV (325 nm)	A_g 3.44 eV (360 nm)
	H−2 → L 0.66641	H−4 → L 0.63212	H−5 → L 0.63311	H−3 → L 0.63581	**H → L+1 0.58895**
4	A_g 3.78 eV (328 nm)	A_g 3.90 eV (318 nm)	A_g 3.96 eV (313 nm)	A_g 3.83 eV (324 nm)	A_u 3.64 eV (340 nm)
	H → L+1 0.54903	H → L+2 0.62891	H → L+2 0.65969	**H → L+1 0.61874**	H → L+2 0.57655

n of S_n	4′mOMe(E)	4′mOMe(Z)
1	A_u 2.1705 eV (571 nm) H → L 0.69033	B_u 2.1682 eV (572 nm) H → L 0.69012
2	A_g 2.9368 eV (422 nm) **H−1 → L** 0.66971	A_g 2.9371 eV (422 nm) **H−1 → L 0.67014**
3	A_g 3.7744 eV (329 nm) H → L+2 0.51137 **H → L+1 −0.40568**	A_g 3.7615 eV (330 nm) **H → L+1 0.48965** H → L+2 −0.42084
4	A_g 3.8763 eV (320 nm) **H → L+1 0.49119** H → L+2 0.4364	A_g 3.8579 eV (321 nm) H → L+2 0.52448 **H → L+1 0.40419**

these differences in the major transition route on the substitution rationalizes the complex shape of the TPA spectra for these dyes.

Molecular Orbital Picture. The nature of the TPA transitions can be understood by examining the electron distribution of the molecular orbital (MO) relating to them. The spectral simulation is based on the sum-overstate (SOS) formalism with summing all intermediate states considered in the calculation (15 excited state and the ground state). Detailed inspection clarified that the transition path via S_1 as the intermediate state is dominant for each TPA transition (Table S1, Supporting Information). From the electronic configuration of the excited states (Table 4), it was found that the moderate or weak $S_0 \rightarrow S_2$ transition (type I) originates from the HOMO−1 → LUMO transition and the intense $S_0 \rightarrow S_f$ transition (f = 3 or higher, depending on the substitution) originates from the HOMO → LUMO+1 transition (type II). Hereafter, we limit the discussion to understand the substitution effect of the type I ($S_0 \rightarrow S_2$) transition to avoid the influence of the complex configuration interaction (CI) among MOs.

DOI: 10.1021/acs.joc.7b00831
J. Org. Chem. 2017, 82, 7254−7264

Since S_1 is the dominant intermediate state, the type I transition can be written as $S_0 \rightarrow S_1 \rightarrow S_2$ and the corresponding electronic transition is HOMO−1 → HOMO → LUMO. The transition dipole moment of $S_0 \rightarrow S_1$, thus, depends on the overlap between HOMO and LUMO while the transition dipole moment between the excited states ($S_1 \rightarrow S_2$) depends on the overlap between HOMO−1 and HOMO. In Figure 6, the patterns of HOMO−1, HOMO, and LUMO for

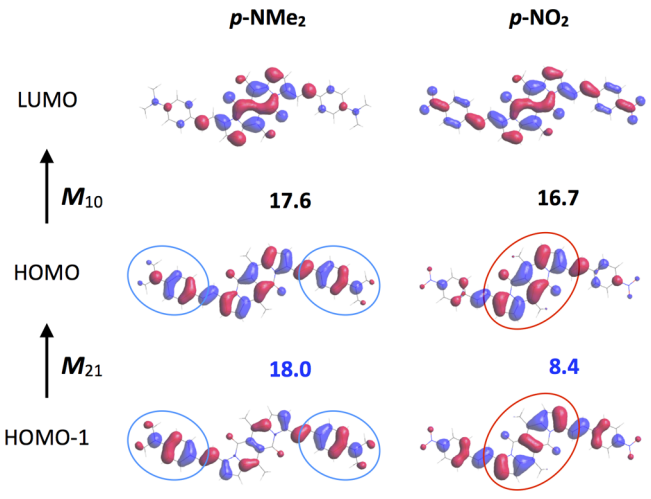

Figure 6. Molecular orbitals related to the type I ($S_0 \rightarrow S_2$) transition of **4′pNMe$_2$** (left column) and **4′pNO$_2$** (right column). The numbers between the orbitals are magnitudes of the corresponding transition dipole moments in units of debye.

the two extreme cases (**4′pNMe$_2$** and **4′pNO$_2$**) are shown. For **4′pNMe$_2$**, a higher density of the electron distribution exists in both substituent groups rather than in the DPND core in HOMOs because of the electron-donating ability of NMe_2 group. Contrary to this, the density is localized in the core for **4′pNO$_2$**, because of the electron-deficient nature of the NO_2 group and the ambipolar character of the DPND core. The transition dipole moment is defined as the product of the distance from the center of the molecule and the charge, so the large distribution at the peripheral groups gives rise to a large transition dipole moment. It turned out that the transition dipole moment between HOMO−1 and HOMO is larger for **4′pNMe$_2$** (18.0 D) than that for **4′pNO$_2$** (8.4 D). On the other hand, the transition dipole moment between HOMO and LUMO is almost the same both for **4′pNMe$_2$** (17.6 D) and for **4′pNO$_2$** (16.7 D). This is because the change of the distribution is opposite for LUMO; i.e., the distribution is localized in the core for **4′pNMe$_2$** and in the substituents for **4′NO$_2$**. The opposite change of HOMO and LUMO by changing the electron-donating/-withdrawing ability of the substituent compensates one another. For other substituents with the same and other linkers, the trend is the same (Figure S5, Supporting Information). As a result, M_{12}, the transition dipole moment of the $S_1 \rightarrow S_2$ transition (HOMO−1 → HOMO), gradually decreases by decreasing the electron-donating ability and increasing the electron-withdrawing ability, while M_{01}, the transition dipole moment of the $S_0 \rightarrow S_1$ transition (HOMO → LUMO), stays unchanged. Since the TPA cross section is proportional to $|M_{01}|^2|M_{12}|^2$ in the SOS fomalism, the TPA peak intensity decreased from the donor to acceptor, as found in Figure 5. The change of the energy detuning, which is another factor contributing to the magnitude of theTPA cross section, was negligible, as shown in Table S1 of the Supporting Information. Thus, it is concluded that the change in the transition dipole moment between the excited states, mostly originating from the electron distribution of HOMOs for DPNDs flanked with substituents possessing different electron-donating/withdrawing ability, determines the behavior of the type I TPA transition.

As for the substituent-position effect between the meta and para positions with the OMe group, the simulated TPA spectrum of **4′pOMe** has a slightly higher peak than that of **4′mOMe(E)/(Z)** at 830 nm (Figure 4). This peak originates from type I (HOMO−1 → LUMO) transitions (Figure 5). In the same manner as discussed above, **4′pOMe** has higher electron density at the substituents, especially at the oxygen atom of the OMe group, in its HOMOs than **4′mOMe(E)/(Z)**, which does not have electron density on the oxygen of the OMe groups (Figure S7, Supporting Information). This difference in the electron distribution matches with the resonance theory, i.e., para-substitution links the π-conjugation between the connecting groups but meta-substitution does not. This change of the electron distribution in HOMOs leads to the change of the transition dipole moments between the excited states (M_{12} = 13.9 D for the para isomer and 12.6 D for both meta isomers). On the other hand, again, the transition dipole moments of $S_0 \rightarrow S_1$ (M_{01} = 15.7 D for the para isomer and 15.6 and 15.5 D for the meta isomers) and the detuning energy (0.72 eV for the para isomer and 0.70 D for both meta isomers) are unvaried. Therefore, the higher TPA cross-section induced by the para-substitution compared to meta-substitution can be explained by the extended π-conjugation to the oxygen atom in the para position through the increased M_{12} of the type I transition.

In addition to the TPA properties, the results of MO calculation also give an insight into the strange trend of the red shift of the first OPA peak, which occurs from donor to acceptor for the ethylene π-linker molecules, i.e., from **4c** (*p*-OMe) to **4a** (*p*-CN) and to **4b** (*p*-NO_2) in Figure 2, but the order is reversed for the ethynylene π-linker molecules, i.e., from **5a** (*p*-NO_2) to **5b** (*p*-OMe) and to **5c** (*p*-NMe_2). The first OPA peaks are assigned to the transitions to S_1, having A_u symmetry. The energy level of S_1 is lowered from the nonsubstituted to the substituted with either strong donor or acceptor, regardless of the direction because of the charge transfer interaction in polar solvent (Table 4). However, the same choice of substituents for the model molecules gave the same trend—565 nm (**4′pOMe**) ⇒ 577 nm (**4′pCN**) ⇒ 589 nm (**4′pNO$_2$**) and 544 nm (**5′pNO$_2$**) ⇒ 548 nm (**5′pOMe**) ⇒ 581 nm (**5′pNMe$_2$**)—although the most-blue-shifted peaks exist in the middle of the donor−acceptor series. Thus, it is naturally concluded that the strange trend observed was eventually caused by the choice of the substituent.

■ CONCLUSIONS

The strategy of enhancing electronic communication by introducing a double bond linkage, instead of a triple bond, between a dipyrrolonaphthyridinedione (DPND) central core and peripheral either electron-donating or electron-accepting groups has been successfully realized. These novel dyes bearing a double bond linkage generally exhibit both absorption and emission bands that are bathochromically shifted to the far-red/NIR region and lower fluorescence quantum yields compared to their analogs with a triple bond linkage. We have shown that, generally, peripheral units containing electron-withdrawing

DOI: 10.1021/acs.joc.7b00831
J. Org. Chem. 2017, 82, 7254−7264

groups are highly desirable to achieve high values of TPA cross sections and, hence, a beneficial ratio of σ_2/MW. Furthermore, compounds bearing triple bond linkages possess high values of two-photon brightness ($\sigma_2 \cdot \Phi_{fl}$), thanks to relatively high values of fluorescence quantum yields. Theoretical calculations revealed that the main TPA band located in the range of 720−860 nm is caused by a OPA-forbidden but TPA-allowed transition to S_2, which is a type I (HOMO−1 → LUMO) transition and is enhanced by increasing the electron distribution on the peripheral substituents of HOMO and HOMO−1 by the electron-donating ability of them. On the other hand, the high TPA cross section for the electron-withdrawing groups is by a type II (HOMO → LUMO+1) transition. The TPA properties (the wavelength position and the magnitude of the peaks) of the symmetric π-extended DPND can be comprehensively understood by the different contributions of type I and II, depending the substituent and the π-linker.

EXPERIMENTAL SECTION

General Remarks. All reagents and solvents were purchased from commercial sources and were used as received, unless otherwise noted. Reagent grade solvents (CH_2Cl_2, hexanes) were distilled prior to use. DMF was dried over phosphorus(V) oxide and then distilled and stored under argon. Transformations with moisture- and oxygen-sensitive compounds were performed under a stream of argon. The reaction progress was monitored by means of thin-layer chromatography (TLC), which was performed on aluminum foil plates, covered with silica gel 60 F254 or aluminum oxide 60 F254 (neutral). Product purifications were done by means of column chromatography with Kieselgel 60 or aluminum oxide. The identity and purity of prepared compounds were proved by ^{1}H NMR and ^{13}C NMR spectrometry as well as by mass spectrometry [HRMS (ESI-TOF) and HRMS (EI); double-focusing magnetic sector instruments with EBE geometry were utilized]. NMR spectra were measured on 400 or 500 MHz instruments with TMS as internal standard. All chemical shifts are given in ppm. All melting points for crystalline products were measured with an automated melting point apparatus and are given without correction. Compounds **1** and **5a−5c** were synthesized as described earlier.[29]

*6,12-Diundecyl-5H,11H-dipyrrolo[1,2-b:1′,2′-g][2,6]-naphthyridine-5,11-dione (**2**).* 1,4-Di(pyrrol-1-yl)butane-1,4-dione[29] (**1**) (1.08 g, 5 mmol, 1.0 equiv) was dissolved in 30 mL of dry dichloromethane under an argon atmosphere, and the solution was cooled to 0 °C. Trifluoroacetic anhydride (12.6 g, 60 mmol, 8.3 mL, 12.0 equiv), trifluoroacetic acid (3.42 g, 30 mmol, 2.3 mL, 6.0 equiv), and lauric acid (6.0 g, 30 mmol, 6.0 equiv) were added, and the resulting mixture was stirred at 0 °C for 10 min and then at room temperature for 3 h. The reaction mixture was then poured into a beaker containing 50 mL of saturated aqueous $NaHCO_3$ and mixed (CO_2 gas evolved). When the evolution of carbon dioxide was no longer observed, the layers were separated. The aqueous layer was extracted three times with chloroform, and the combined organic layers were washed with water and dried over $MgSO_4$. Product was purified using column chromatography (SiO_2, *n*-hexane:dichloromethane 2:1) and recrystallized from ethyl acetate. Compound **2** (653.8 mg, 24% yield) was obtained as a red solid. R_f = 0.44 (SiO_2, *n*-hexane:DCM 2:1). Mp: 99−101 °C. ^{1}H NMR (400 MHz, $CDCl_3$): δ 7.84 (dd, 2H, J_1 = 3.2 Hz, J_2 = 1.2 Hz, pyrrole H), 6.87 (dd, 2H, J_1 = 3.6 Hz, J_2 = 1.2 Hz, pyrrole H), 6.54 (t, 2H, J = 3.6 Hz, pyrrole H), 3.30−3.26 (m, 4H, $CH_2(CH_2)_5CH_3$), 1.71−1.65 (m, 4H, $CH_2(CH_2)_5CH_3$), 1.56−1.49 (m, 4H, $CH_2(CH_2)_5CH_3$), 1.39−1.27 (m, 28H, $CH_2(CH_2)_5CH_3$), 0.88 (t, 6H, J = 7.2 Hz, $CH_2(CH_2)_5CH_3$). ^{13}C NMR (125 MHz, $CDCl_3$): δ 158.4, 145.5, 133.2, 122.5, 116.5, 115.4, 114.4, 31.9, 31.1, 30.4, 30.3, 29.7, 29.6, 29.6, 29.5, 29.3, 22.7, 14.1. HRMS (EI) m/z: [$M^{\bullet+}$] calcd for $C_{36}H_{52}N_2O_2$ 544.4029, found 544.4020. Anal. Calcd for $C_{36}H_{52}N_2O_2$: C, 79.36; H, 9.62; N, 5.14. Found: C, 79.44; H, 9.78; N, 5.16.

*3,9-Dibromo-6,12-diundecyl-5H,11H-dipyrrolo[1,2-b:1′,2′-g][2,6]-naphthyridine-5,11-dione (**3**).* A solution of **2** (545 mg, 1 mmol, 1.0 equiv) in 15 mL of chloroform was stirred at 0 °C (water−ice bath). Freshly recrystallized *N*-bromosuccinimide (374 mg, 2.1 mmol, 2.1 equiv) was added and the obtained mixture was stirred in darkness (protection with aluminum foil) for 16 h. During this time, the ice in the ice bath melted and the reaction mixture warmed to room temperature. The reaction mixture was diluted with chloroform, washed with water three times, and dried over $MgSO_4$. Product was purified using column chromatography (SiO_2, *n*-hexane:dichloromethane 2:1) and recrystallized from ethyl acetate. Compound **3** (386 mg, 55% yield) was obtained as a dark brown powder. R_f = 0.55 (SiO_2, *n*-hexane:DCM 2:1). Mp: 125−127 °C. ^{1}H NMR (400 MHz, $CDCl_3$): δ 6.81 (d, 2H, J = 4.0 Hz, pyrrole H), 6.58 (d, 2H, J = 4.0 Hz, pyrrole H), 3.19−3.15 (m, 4H, $CH_2(CH_2)_5CH_3$), 1.70−1.63 (m, 4H, $CH_2(CH_2)_5CH_3$), 1.54−1.47 (m, 4H, $CH_2(CH_2)_5CH_3$), 1.36−1.27 (m, 28H, $CH_2(CH_2)_5CH_3$), 0.88 (t, 6H, J = 7.2 Hz, $CH_2(CH_2)_5CH_3$). ^{13}C NMR (125 MHz, $CDCl_3$): δ 158.8, 143.3, 134.9, 120.5, 115.8, 115.3, 106.5, 31.9, 30.2, 30.2, 29.7, 29.6, 29.6, 29.5, 29.3, 22.7, 14.1. HRMS (EI) m/z: [$M^{\bullet+}$] calcd for $C_{36}H_{50}N_2O_2Br_2$ 700.2239, found 700.2236. Anal. Calcd for $C_{36}H_{50}N_2O_2Br_2$: C, 61.54; H, 7.17; N, 3.99; Br, 22.74. Found: C, 61.69; H, 6.97; N, 4.10; Br, 22.84.

General Procedure for the Synthesis of 4a−4c. In a Schlenk flask containing a magnetic stirring bar were placed **3** (0.1 mmol, 70.2 mg, 1.0 equiv), palladium(II) acetate (2.2 mg, 0.01 mmol, 10 mol %), and tri(*o*-tolyl)phosphine (6.1 mg, 0.02 mmol, 20 mol %). The vessel was evacuated and backfilled with argon (three times) and anhydrous, degassed DMF was added (6 mL) followed by argonated $(i\text{-Pr})_2$NEt (DIPEA) (0.1 mL) and styrene (0.4 mmol, 4.0 equiv). The vessel was tightly closed and again carefully evacuated and backfilled with argon (three times). The contents of the flask were stirred at 90 °C for 24 h. All volatiles were evaporated and the product was purified as described below.

*3,9-Bis((E)-4-cyanostyryl)-6,12-diundecyl-5H,11H-dipyrrolo[1,2-b:1′,2′-g][2,6]naphthyridine-5,11-dione (**4a**).* The title compound was prepared from 4-cynanostyrene (51.7 mg, 51.7 μL, 0.4 mmol). The product was purified using column chromatography (SiO_2, *n*-hexane:dichloromethane 1:1 then 1:2) and recrystallized by slow addition of methanol to a hot solution of the dye in a small amount of chloroform. Compound **4a** (44.7 mg, 56% yield) was obtained as dark brown crystals. R_f = 0.37 (SiO_2, *n*-hexane:DCM 1:2). Mp: 321−323 °C. ^{1}H NMR (500 MHz, $CDCl_3$): δ 8.50 (d, 2H, J = 13.2 Hz, CH_2=CH_2), 7.63 (m, 8H, Ar−H), 7.06 (d, 2H, J = 16.4 Hz, CH_2=CH_2), 6.95 (d, 2H, J = 4.0 Hz, pyrrole H), 6.91 (d, 2H, J = 4.1 Hz, pyrrole H), 3.27−3.24 (m, 4H, $CH_2(CH_2)_5CH_3$), 1.71−1.68 (m, 4H, $CH_2(CH_2)_5CH_3$), 1.58−1.53 (m, 4H, $CH_2(CH_2)_5CH_3$), 1.42−1.40 (m, 4H, $CH_2(CH_2)_5CH_3$) 1.32−1.27 (m, 24H, $CH_2(CH_2)_5CH_3$), 0.88 (t, 6H, J = 6.5 Hz, $CH_2(CH_2)_5CH_3$). ^{13}C NMR (125 MHz, $CDCl_3$): δ 160.7, 143.3, 141.7, 138.9, 135.5, 132.5, 128.9, 127.1, 123.4, 119.0, 116.7, 115.8, 114.9, 110.7, 31.9, 30.7, 30.5, 30.3, 29.7, 29.7, 29.5, 29.4, 22.7, 14.1. HRMS (EI) m/z: [$M^{\bullet+}$] calcd for $C_{54}H_{62}N_4O_2$ 798.4873, found 798.4851.

*3,9-Bis((E)-4-nitrostyryl)-6,12-diundecyl-5H,11H-dipyrrolo[1,2-b:1′,2′-g][2,6]naphthyridine-5,11-dione (**4b**).* The title compound was prepared from 4-nitrostyrene (59.7 mg, 51.3 μL, 0.4 mmol). The product was purified using column chromatography (SiO_2, cyclohexane:dichloromethane 2:3) and recrystallized twice from toluene. Compound **4b** (15.1 mg, 18% yield) was obtained as dark brown crystals. R_f = 0.47 (SiO_2, cyclohexane:DCM, 2:3). Mp: >400 °C. ^{1}H NMR (500 MHz, $CDCl_3$, 50 °C): δ 8.55 (d, 2H, J = 16.5 Hz, CH_2=CH_2), 8.22 (d, 4H, J = 8.5 Hz, Ar−H), 7.66 (d, 4H, J = 8.5 Hz, Ar−H), 7.10 (d, 2H, J = 16.5 Hz, CH_2=CH_2), 6.97 (d, 2H, J = 3.5 Hz, pyrrole H), 6.92 (d, 2H, J = 4.0 Hz, pyrrole H), 3.30−3.26 (m, 4H, $CH_2(CH_2)_5CH_3$), 1.75−1.70 (m, 4H, $CH_2(CH_2)_5CH_3$), 1.60−1.54 (m, 4H, $CH_2(CH_2)_5CH_3$), 1.47−1.41 (m, 4H, $CH_2(CH_2)_5CH_3$), 1.34−1.26 (m, 24H, $CH_2(CH_2)_5CH_3$), 0.87 (t, 6H, J = 7.0 Hz, $CH_2(CH_2)_5CH_3$). ^{13}C NMR (125 MHz, $CDCl_3$, 50 °C): δ 160.7, 147.0, 143.7, 143.4, 138.8, 135.7, 128.4, 127.0, 124.2, 124.1, 116.6,

DOI: 10.1021/acs.joc.7b00831
J. Org. Chem. 2017, 82, 7254−7264

116.0, 115.0, 31.8, 30.6, 30.4, 30.2, 29.7, 29.6, 29.6, 29.4, 29.3, 22.6, 13.9. HRMS (EI) m/z: [$M^{\bullet+}$] calcd for $C_{52}H_{62}N_4O_6$ 838.4669, found 838.4640.

*3,9-Bis((E)-3-methoxystyryl)-6,12-diundecyl-5H,11H-dipyrrolo-[1,2-b:1′,2′-g][2,6]naphthyridine-5,11-dione (**4c**).* The title compound was prepared from 3-methoxystyrene (53.7 mg, 55.5 μL, 0.4 mmol). The product was purified using column chromatography (SiO_2, cyclohexane:dichloromethane 3:2). The obtained fraction was evaporated off and washed with methanol until the washings were colorless to give a sufficiently pure compound. Compound **4c** (41.3 mg, 51% yield) was obtained as a dark violet powder. R_f = 0.32 (SiO_2, cyclohexane:DCM 3:2). Mp: 173−175 °C. ^{1}H NMR (500 MHz, CD_2Cl_2): δ 8.35 (d, 2H, J = 13.2 Hz, CH_2═CH_2), 7.30 (t, 2H, J = 6.0 Hz, Ar−H), 7.17 (d, 2H, J = 6.0 Hz, Ar−H), 7.08 (m, 4H, CH_2═CH_2 + pyrrole H), 6.92 (m, 4H, Ar−H + pyrrole H), 6.84 (d, 2H, J = 8.0 Hz, Ar−H), 3.85 (s, 6H, OMe), 3.27−3.24 (m, 4H, $CH_2(CH_2)_5CH_3$), 1.70 (m, 4H, $CH_2(CH_2)_5CH_3$), 1.57−1.54 (m, 4H, $CH_2(CH_2)_5CH_3$), 1.42−1.28 (m, 28H, $CH_2(CH_2)_5CH_3$), 0.88 (t, 6H, J = 5.6 Hz, $CH_2(CH_2)_5CH_3$). ^{13}C NMR (125 MHz, CD_2Cl_2): δ 171.9, 161.3, 160.5, 143.1, 140.0, 139.2, 135.4, 131.2, 130.0, 120.8, 119.7, 116.8, 115.9, 114.3, 113.9, 112.5, 55.6, 32.3, 31.0, 30.9, 30.7, 30.1, 30.1, 29.9, 29.8, 23.1, 14.3. HRMS (EI) m/z: [$M^{\bullet+}$] calcd for $C_{54}H_{68}N_2O_4$ 808.5179, found 808.5165.

Optical Measurements. For the measurements of absorption and emission spectra, a typical UV/vis spectrophotometer and a spectrofluorimeter were used. Dichloromethane was spectrophotometric grade and was used without further purification. Quartz cells (10 mm) were used for the measurements of absorption and emission spectra. As a standard, cresyl violet was used to determine fluorescence quantum yields (Φ_{fl} = 0.54 in MeOH).

Two-Photon Absorption Measurements. The Z-scan setup used for the TPA spectral measurements was reported previously.[36] A femtosecond optical parametric amplifier (SpectraPhysics TOPAS-Prime pumped by a Ti:sapphire regenerative amplifier operating at 1 kHz) was used as the light source (typical pulse width of 120 fs). Different optical configurations of the optical parametric amplifier were used depending on the wavelength regions. The second harmonic of the signal (SHS) was used for 720−800 nm and the second harmonic of the idler (SHI) was used for 820−960 nm. The sample solution prepared in dichloromethane was held in a quartz cuvette with the path length of 2 mm, which was short enough to hold the thin-sample condition against the Rayleigh range of the setup (7−10 mm depending on the wavelength). The observed open-aperture Z-scan traces were analyzed by the curve-fitting procedure assuming the spatial and temporal Gaussian distributions of the optical intensity of the incident laser pulses.[36] All sample solutions were stirred during the measurements because the probable TPA-induced photoreaction of the observed volume was observed. The incident power was set below 0.5 mW, corresponding to the on-axis optical intensity of 150−200 GW/cm^2 at the focal position, depending on the wavelength and the Rayleigh range. The concentrations of the sample solutions employed were around 1 mM except for **4a**, **4b**, and **5a** (∼0.2, ∼0.1, and ∼0.2 mM, respectively) because of the poor solubility in dichloromethane.

■ ASSOCIATED CONTENT

Supporting Information

The Supporting Information is available free of charge on the ACS Publications website at DOI: 10.1021/acs.joc.7b00831.

Absorption and normalized emission spectra of compounds **4a**−**4c** and **5a**−**5c**; ^{1}H NMR and ^{13}C NMR spectra for compounds **2**, **3**, and **4a**−**4c**; and detailed information about TPA measurements as well as theoretical calculations (PDF)

■ AUTHOR INFORMATION

Corresponding Authors

*E-mail for K.K.: k.kamada@aist.go.jp.

*E-mail for D.T.G.: dtgryko@icho.edu.pl.

ORCID

Daniel T. Gryko: 0000-0002-2146-1282

Notes

The authors declare no competing financial interest.

■ ACKNOWLEDGMENTS

The work was financially supported by the Polish National Science Centre (grant MAESTRO-2012/06/A/ST5/00216 and PRELUDIUM 2016/23/N/ST5/00054), and by the Global Research Laboratory Program (2014K1A1A2064569) through the National Research Foundation (NRF) funded by the Ministry of Science, ICT & Future Planning (Korea). This work was also partially supported by JSPS KAKENHI Grant Number JP15H00966, JP25248007, JP26288016, JP26107004 (K.K.).

■ REFERENCES

(1) (a) Denk, W.; Strickler, J. H.; Webb, W. W. *Science* **1990**, *248*, 73−76. (b) Marder, S. R. *Chem. Commun.* **2006**, 131−134.

(2) (a) Qian, L.; Zhang, C.-W.; Mao, Y.; Li, L.; Gao, N.; Lim, K.-L.; Xu, Q.-H.; Yao, S. Q. *Sci. Rep.* **2016**, *6*, 26385. (b) Wang, K.; Horton, N. G.; Xu, C. *Opt. Photonics News* **2013**, *24*, 32−39.

(3) (a) Griesbeck, S.; Zhang, Z.; Gutmann, M.; Léhmann, T.; Edkins, R. M.; Clermont, G.; Lazar, A. N.; Haehnel, M.; Edkins, K.; Eichhorn, A.; Blanchard-Desce, M.; Meinel, L.; Marder, T. B. *Chem. - Eur. J.* **2016**, *22*, 14701−14706. (b) Sarkar, A. R.; Heo, C. H.; Lee, H. W.; Park, K. H.; Suh, Y. H.; Kim, H. M. *Anal. Chem.* **2014**, *86*, 5638−5641.

(4) (a) Sui, H.; Yue, X.; Kim, B.; Belfield, K. D. *ACS Appl. Mater. Interfaces* **2015**, *7*, 17565−17568. (b) Lee, H.-J.; Cho, C.-W.; Seo, H.; Singha, S.; Jun, Y. W.; Lee, K.-H.; Jung, Y.; Kim, K.-T.; Park, S.; Bae, S. C.; Ahn, K. H. *Chem. Commun.* **2016**, *52*, 124−127.

(5) (a) Das, S. K.; Lim, C. S.; Yang, S. Y.; Han, J. H.; Cho, B. R. *Chem. Commun.* **2012**, *48*, 8395−8397. (b) Sun, W.; Fan, J.; Hu, C.; Cao, J.; Zhang, H.; Xiong, X.; Wang, J.; Cui, S.; Sun, S.; Peng, X. *Chem. Commun.* **2013**, *49*, 3890−3892. (c) Bae, S. K.; Heo, C. H.; Choi, D. J.; Sen, D.; Joe, E. H.; Cho, B. R.; Kim, H. M. *J. Am. Chem. Soc.* **2013**, *135*, 9915−9923.

(6) (a) Seo, E. W.; Han, J. H.; Heo, C. H.; Shin, J. H.; Kim, H. M.; Cho, B. R. *Chem. - Eur. J.* **2012**, *18*, 12388−12394. (b) Yu, H.; Xiao, Y.; Jin, L. *J. Am. Chem. Soc.* **2012**, *134*, 17486−17489.

(7) (a) Chang, M. C. Y.; Pralle, A.; Isacoff, E. Y.; Chang, C. J. *J. Am. Chem. Soc.* **2004**, *126*, 15392−15393. (b) Chung, C.; Srikun, D.; Lim, C. S.; Chang, C. J.; Cho, B. R. *Chem. Commun.* **2011**, *47*, 9618−9620.

(8) Kim, D.; Moon, H.; Baik, S. H.; Singha, S.; Jun, Y. W.; Wang, T.; Kim, K. H.; Park, B. S.; Jung, J.; Mook-Jung, I.; Ahn, K. H. *J. Am. Chem. Soc.* **2015**, *137*, 6781−6789.

(9) (a) Lee, J. H.; Lim, C. S.; Tian, Y. S.; Han, J. H.; Cho, B. R. *J. Am. Chem. Soc.* **2010**, *132*, 1216−1217. (b) Yang, Z.; Zhao, N.; Sun, Y.; Miao, F.; Liu, Y.; Liu, X.; Zhang, Y.; Ai, W.; Song, G.; Shen, X.; Yu, X.; Sun, J.; Wong, W. *Chem. Commun.* **2012**, *48*, 3442−3444. (c) Zhang, X.; Ren, X.; Xu, Q.; Loh, K. P.; Chen, Z. *Org. Lett.* **2009**, *11*, 1257−1260.

(10) (a) Fisher, W. G.; Partridge, W. P., Jr.; Dees, C.; Wachter, E. A. *Photochem. Photobiol.* **1997**, *66*, 141−155. (b) Shen, Y.; Shuhendler, A. J.; Ye, D.; Xu, J.-J.; Chen, H.-Y. *Chem. Soc. Rev.* **2016**, *45*, 6725−6741.

(11) (a) Juodkazis, S.; Mizeikis, V.; Misawa, H. *J. Appl. Phys.* **2009**, *106*, 051101. (b) Sekkat, Z.; Kawata, S. *Laser&Photon. Rev.* **2014**, *8*, 1−26. (c) Nazir, R.; Danilevicius, P.; Ciuciu, A. I.; Chatzinikolaidou, M.; Gray, D.; Flamigni, L.; Farsari, M.; Gryko, D. T. *Chem. Mater.* **2014**, *26*, 3175−3184. (d) Xing, J.-F; Zheng, M.-L.; Duan, X.-M. *Chem. Soc. Rev.* **2015**, *44*, 5031−5039.

(12) (a) Spangler, C. W. *J. Mater. Chem.* **1999**, *9*, 2013−2020. (b) Kumaresan, P.; Liu, Y. Y.; Vegiraju, S.; Ezhumalai, Y.; Yu, H. C.; Yau, S. L.; Chen, M. C.; Lin, T. C. *Chem. - Asian J.* **2015**, *10*, 1640−1646.

DOI: 10.1021/acs.joc.7b00831
J. Org. Chem. 2017, 82, 7254−7264

(13) Rebane, A.; Wicks, G.; Drobizhev, M.; Cooper, T.; Trummal, A.; Uudsemaa, M. *Angew. Chem., Int. Ed.* **2015**, *54*, 7582−7586.
(14) (a) Parthenopoulos, D. A.; Rentzepis, P. M. *Science* **1989**, *245*, 843−845. (b) Kawata, S.; Kawata, Y. *Chem. Rev.* **2000**, *100*, 1777−1788. (c) Dallari, W.; Scotto, M.; Allione, M.; Samoylova, E.; Pignatelli, F.; Cingolani, R.; Athanassiou, A.; Diaspro, A. *Microelectron. Eng.* **2011**, *88*, 3466−3469.
(15) (a) Fischer, J.; von Freymann, G.; Wegener, M. *Adv. Mater.* **2010**, *22*, 3578−3582. (b) Ushiba, S.; Shoji, S.; Masui, K.; Kuray, P.; Kono, J.; Kawata, S. *Carbon* **2013**, *59*, 283−288.
(16) (a) Pond, S. J. K.; Tsutsumi, O.; Rumi, M.; Kwon, O.; Zojer, E.; Brédas, J.-L.; Marder, S. R.; Perry, J. W. *J. Am. Chem. Soc.* **2004**, *126*, 9291−9306. (b) Albota, M.; Beljonne, D.; Brédas, J.-L.; Ehrlich, J. E.; Fu, J.-Y.; Heikal, A. A.; Hess, S. E.; Kogej, T.; Levin, M. D.; Marder, S. R.; McCord-Maughon, D.; Perry, J. W.; Röckel, H.; Rumi, M.; Subramaniam, G.; Webb, W. W.; Wu, X.-L; Xu, C. *Science* **1998**, *128*, 1653−1656.
(17) (a) Mongin, O.; Porrés, L.; Moreaux, L.; Mertz, J.; Blanchard-Desce, M. *Org. Lett.* **2002**, *4*, 719−722. (b) Belfield, K. D.; Schafer, K. J.; Mourad, W.; Reinhardt, B. A. *J. Org. Chem.* **2000**, *65*, 4475−4481. (c) Charlot, M.; Izard, N.; Mongin, O.; Riehl, D.; Blanchard-Desce, M. *Chem. Phys. Lett.* **2006**, *417*, 297−302. (d) Mongin, O.; Porrés, L.; Charlot, M.; Katan, C.; Blanchard-Desce, M. *Chem. - Eur. J.* **2007**, *13*, 1481−1489.
(18) Kim, D.; Xuan, Q. P.; Moon, H.; Jun, Y. W.; Ahn, K. H. *Asian J. Org. Chem.* **2014**, *3*, 1089−1096.
(19) (a) Ahn, T. K.; Kim, K. S.; Kim, D. Y.; Noh, S. B.; Aratani, N.; Ikeda, C.; Osuka, A.; Kim, D. *J. Am. Chem. Soc.* **2006**, *128*, 1700−1704. (b) Collins, H. A.; Khurana, M.; Moriyama, E. H.; Mariampillai, A.; Dahlstedt, E.; Balaz, M.; Kuimova, M. K.; Drobizhev, M.; Yang, V. X. D.; Phillips, D.; Rebane, A.; Wilson, B. C.; Anderson, H. L. *Nat. Photonics* **2008**, *2*, 420−424.
(20) Kamada, K.; Fuku-en, S.; Minamide, S.; Ohta, K.; Kishi, R.; Nakano, M.; Matsuzaki, H.; Okamoto, H.; Higashikawa, H.; Inoue, K.; Kojima, S.; Yamamoto, Y. *J. Am. Chem. Soc.* **2013**, *135*, 232−241.
(21) Orian, L.; Scuppa, S.; Santi, S.; Meneghetti, M. *Phys. Chem. Chem. Phys.* **2013**, *15*, 12971−12976.
(22) (a) Lin, T. C.; He, G. S.; Prasad, P. N.; Tan, L. S. *J. Mater. Chem.* **2004**, *14*, 982−991. (b) Beverina, L.; Fu, J.; Leclercq, A.; Zojer, E.; Pacher, P.; Barlow, S.; Van Stryland, E. W.; Hagan, D. J.; Bredas, J. L.; Marder, S. R. *J. Am. Chem. Soc.* **2005**, *127*, 7282−7283. (c) Kim, H. M.; Fang, X. Z.; Yang, P. R.; Yi, J. S.; Ko, Y. G.; Piao, M. J.; Chung, Y. D.; Park, Y. W.; Jeon, S. J.; Cho, B. R. *Tetrahedron Lett.* **2007**, *48*, 2791−2795.
(23) (a) Rumi, M.; Ehrlich, J. E.; Heikal, A. A.; Perry, J. W.; Barlow, S.; Hu, Z. Y.; McCord-Maughon, D.; Parker, T. C.; Rockel, H.; Thayumanavan, S.; Marder, S. R.; Beljonne, D.; Bredas, J. L. *J. Am. Chem. Soc.* **2000**, *122*, 9500−9510. (b) Chung, S. J.; Zheng, S. J.; Odani, T.; Beverina, J.; Fu, L.; Padilha, L. A.; Biesso, A.; Hales, J. M.; Zhan, X.; Schmidt, K.; Ye, A. J.; Zojer, E.; Barlow, S.; Hagan, D. J.; Van Stryland, E. W.; Yi, Y. P.; Shuai, Z. G.; Pagani, G. A.; Bredas, J. L.; Perry, J. W.; Marder, S. R. *J. Am. Chem. Soc.* **2006**, *128*, 14444−14445.
(24) (a) Shao, J.; Guan, Z.; Yan, Y.; Jiao, C.; Xu, Q.-X.; Chi, C. *J. Org. Chem.* **2011**, *76*, 780−790. (b) Hrobárik, P.; Hrobáriková, V.; Sigmundová, I.; Zahradník, P.; Fakis, M.; Polyzos, I.; Persephonis, P. *J. Org. Chem.* **2011**, *76*, 8726−8736. (c) Jędrzejewska, B.; Gordel, M.; Szeremeta, J.; Krawczyk, P.; Samoć, M. *J. Org. Chem.* **2015**, *80*, 9641−9651. (d) Poronik, Y. M.; Hugues, V.; Blanchard-Desce, M.; Gryko, D. T. *Chem. - Eur. J.* **2012**, *18*, 9258−9266.
(25) (a) Pawlicki, M.; Collins, H. A.; Denning, R. G.; Anderson, H. L. *Angew. Chem., Int. Ed.* **2009**, *48*, 3244−3266. (b) Kim, H. M.; Cho, B. R. *Chem. Commun.* **2009**, 153−164.
(26) (a) Yang, W. J.; Kim, D. Y.; Jeong, M. Y.; Kim, H. M.; Lee, Y. K.; Fang, X.; Jeon, S. J.; Cho, B. R. *Chem. - Eur. J.* **2005**, *11*, 4191−4198. (b) Yang, W. J.; Kim, D. Y.; Jeong, M. Y.; Kim, H. M.; Jeon, S. J.; Cho, B. R. *Chem. Commun.* **2003**, 2618−2619.
(27) Zheng, S. J.; Leclercq, A.; Fu, J.; Beverina, L.; Padilha, L. A.; Zojer, E.; Schmidt, K.; Barlow, S.; Luo, J. D.; Jiang, S. H.; Jen, A. K. Y.; Yi, Y. P.; Shuai, Z. G.; Van Stryland, E. W.; Hagan, D. J.; Bredas, J. L.; Marder, S. R. *Chem. Mater.* **2007**, *19*, 432−442.
(28) Grzybowski, M.; Głodkowska-Mrówka, E.; Hugues, V.; Brutkowski, W.; Blanchard-Desce, M.; Gryko, D. T. *Chem. - Eur. J.* **2015**, *21*, 9101−9110.
(29) Grzybowski, M.; Deperasińska, I.; Chotkowski, M.; Banasiewicz, M.; Makarewicz, A.; Kozankiewicz, B.; Gryko, D. T. *Chem. Commun.* **2016**, *52*, 5108−5111.
(30) (a) Purc, A.; Sobczyk, K.; Sakagami, Y.; Ando, A.; Kamada, K.; Gryko, D. T. *J. Mater. Chem. C* **2015**, *3*, 742−749. (b) Grzybowski, M.; Hugues, V.; Blanchard-Desce, M.; Gryko, D. T. *Chem. - Eur. J.* **2014**, *20*, 12493−12501.
(31) (a) Janiga, A.; Bednarska, D.; Thorsted, B.; Brewer, J.; Gryko, D. T. *Org. Biomol. Chem.* **2014**, *12*, 2874−2881. (b) Stężycki, R.; Grzybowski, M.; Clermont, G.; Blanchard-Desce, M.; Gryko, D. T. *Chem. - Eur. J.* **2016**, *22*, 5198−5203. (c) Friese, D. H.; Mikhaylov, A.; Krzeszewski, M.; Poronik, Y. M.; Rebane, A.; Ruud, K.; Gryko, D. T. *Chem. - Eur. J.* **2015**, *21*, 18364−18374.
(32) Lebel, H.; Janes, M. K.; Charette, A. B.; Nolan, S. P. *J. Am. Chem. Soc.* **2004**, *126*, 5046−5047.
(33) McCartin, P. J. *J. Chem. Phys.* **1965**, *42*, 2980−2981.
(34) (a) Bolduc, A.; Dong, Y.; Guérin, A.; Skene, W. G. *Phys. Chem. Chem. Phys.* **2012**, *14*, 6946−6956. (b) Carlotti, B.; Elisei, F.; Mazzucato, U.; Spalletti, A. *Phys. Chem. Chem. Phys.* **2015**, *17*, 14740−14749. (c) Kotaka, H.; Konishi, G.; Mizuno, K. *Tetrahedron Lett.* **2010**, *51*, 181−184. (d) Hachiya, S.; Asai, K.; Konishi, G. *Tetrahedron Lett.* **2013**, *54*, 1839−1841. (e) Nandhikonda, P.; Heagy, M. D. *Chem. Commun.* **2010**, *46*, 8002−8004.
(35) Sheik-Bahae, M.; Said, A. A.; Wei, T.-H.; Hagan, D. G.; van Stryland, E. W. *IEEE J. Quantum Electron.* **1990**, *26*, 760−769.
(36) Kamada, K.; Matsunaga, K.; Yoshino, A.; Ohta, K. *J. Opt. Soc. Am. B* **2003**, *20*, 529−537.
(37) (a) Meier, H. *Angew. Chem., Int. Ed.* **2005**, *44*, 2482−2506. (b) Mongin, O.; Porrès, L.; Charlot, M.; Katan, C.; Blanchard-Desce, M. *Chem. - Eur. J.* **2007**, *13*, 1481−1498. (c) Kamada, K.; Iwase, Y.; Sakai, K.; Kondo, K.; Ohta, K. *J. Phys. Chem. C* **2009**, *113*, 11469−11474.
(38) Lee, S. K.; Yang, W. J.; Choi, J. J.; Kim, C. H.; Jeon, S. J.; Cho, B. R. *Org. Lett.* **2005**, *7*, 323−326.
(39) Kim, K. S.; Noh, S. B.; Katsuda, T.; Ito, S.; Osuka, A.; Kim, D. *Chem. Commun.* **2007**, 2479−2481.
(40) Hirata, S.; Head-Gordon, M. *Chem. Phys. Lett.* **1999**, *314*, 291−299.
(41) Ohta, K.; Yamada, S.; Kamada, K.; Slepkov, A. D.; Hegmann, F. A.; Tykwinski, R. R.; Shirtcliff, L. D.; Haley, M. M.; Sałek, P.; Gel'mukhanov, F.; Ågren, H. *J. Phys. Chem. A* **2011**, *115*, 105−117.

DOI: 10.1021/acs.joc.7b00831
J. Org. Chem. 2017, 82, 7254−7264